Prod. Eng. Res. Devel. (2009) 3:271–279
DOI 10.1007/s11740-009-0163-3

COMPUTER AIDED ENGINEERING

# Experimental and numerical identification of process parameters of grind-hardening and resulting part distortions

**Michael F. Zäh · Ekkard Brinksmeier · Carsten Heinzel · Jens-Walter Huntemann · Tobias Föckerer**

Received: 27 April 2009 / Accepted: 10 July 2009 / Published online: 31 July 2009


**Abstract** Using the heat input into the workpiece during grinding to simultaneously realize surface hardening is the innovative approach of the grind-hardening process. Due to the complex physical phenomena within this process, the layout requires extensive experimental analysis to handle the surface hardening and the process-related part distortions. This paper presents a method supporting the layout by means of the finite element analysis (FEA). Besides the hardening depth distributions and the resulting distortions, the research results comprise the numerical identification of the range of the grind-hardening process regarding the analyzed parameter sets. Therewith, the FEA provides the possibility to meet the characteristics of the grind-hardening and to support the layout of the process efficiently.

**Keywords** Computer aided engineering · Grind-hardening · Process parameter identification · Part distortion

## 1 Introduction

Grinding is a machining process which allows high dimensional accuracy and surface quality of the machined part as well as high material removal rates. Nevertheless, grinding is predominantly used as a finishing technology after several steps of soft machining and a subsequent heat treatment at the end of the process chain. Such a process chain is characterized by inevitable auxiliary process time as well as costs for stockkeeping and logistics.

An innovative approach is to cut down the process and auxiliary time by substitution of conventional hardening processes with the machining process "grind-hardening". Grind-hardening offers the ability for process integrated surface layer hardening by grinding with a subsequent finishing in one clamping. The large amount of heat in the contact zone between the grinding wheel and the workpiece, which is generated by deformation, shearing, friction and separation while grinding, is used for a surface layer short time austenization of the machined part. The martensitic hardening is mainly achieved by self quenching [1], which is supported by the convective heat transport of the used coolant [2].

To introduce the grind-hardening process within an industrial environment it is necessary to predict the achievable surface hardening and especially the process-related distortions of the machined part. Due to the complex physical interrelationships within this process this prediction is difficult and often requires extensive test series.

An effective method to reduce time and effort for the layout of the grind-hardening process is its modeling and the numerical simulation by means of the finite element analysis (FEA) based on experimental analyses.

The objective of the presented study was to develop a FEA-based simulation method of heat induced distortion during grind-hardening. To evaluate the quality of the used models and methods, the results of the simulations are validated by means of experiments.

M. F. Zäh · T. Föckerer (✉)
Institute for Machine Tools and Industrial Management (iwb), Technische Universitaet Muenchen, Boltzmannstr. 15, 85748 Munich, Germany
e-mail: tobias.foeckerer@iwb.tum.de

E. Brinksmeier · C. Heinzel · J.-W. Huntemann
Foundation Institute of Materials Science (IWT), Badgasteiner Str. 3, 28359 Bremen, Germany

## 2 Experimental analyses

The input data for the simulations are based on the parameters of straight surface grinding tests using a vitrified bonded grinding wheel with corundum abrasive grains and a diameter of 400 mm. All experiments were conducted on an ELB Micro-Cut A8 CNC grinder using an water based coolant solution with a flow rate of 25 l/min. The grinding operations were performed in up cut mode with a wheel speed of $v_c = 35$ m/s. During the tests, the specific material removal rate $Q'_w$ was varied by adjusting the tangential feed rate $v_{ft}$ in the range from 0.18 m/min up to 6.0 m/min and the depth of cut $a_e$ in the range from 0.1 mm up to 1.0 mm. As workpiece material soft-annealed bearing steel 100Cr6 was used.

### 2.1 Measurement of grinding forces and temperature during grind-hardening

The total amount of heat in the contact zone as well as the partition ratio of heat penetrating the workpiece are important factors for the simulation of thermally caused part distortions. Considering that in grinding nearly the entire mechanical energy is converted into heat, the total amount of heat is ascertainable by measurements of the tangential grinding force. Thus, grinding forces were measured during the test series with the setup illustrated in Fig. 1. Additionally, the temperatures in different distances from the contact zone were measured for the evaluation of the quality of the used models and methods.

Before the workpieces, which were 150 mm long in grinding direction, 120 mm wide and 28 mm high, were mounted on a force plate (3-component-dynamometer), they were equipped with five NiCr-Ni mantle thermocouples in different distances to the workpiece surface, shown in Fig. 3. Three thermocouples (TC) were applied in the center of the grinding wheel (TC1, TC3 and TC5), one 3 mm besides the grinding wheel center (TC2) and one 5 mm outside the grinding groove (TC4). The thermocouples, which have a response time of 14 ms, were embedded into blind holes at the bottom side of the workpiece. The distance to the workpiece surface was determined by measuring the blind holes' depth with tactile measurement methods. In further tests, which dealt with the measurement of the temperature in the contact zone, thermocouples were embedded into through holes with a diameter of 0.4 mm. By doing this, the exact position of the thermocouples related to the workpiece surface could be measured by tactile measurement methods after the installation of the thermocouples.

The analogue output from the thermocouples was fed to a microcomputer through a signal conditioning module with a sampling rate of 5 kHz.

Figure 2 shows the tangential and normal grinding force measured during the grind-hardening operation for different parameter sets, whereas Fig. 3 shows exemplarily the

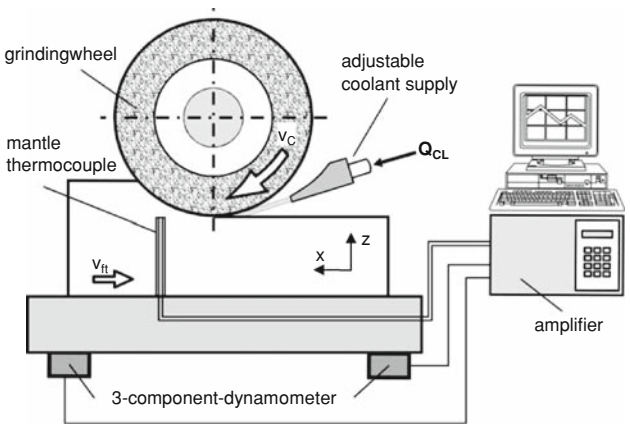


**Fig. 1** Illustration of the setup for force and temperature measurements

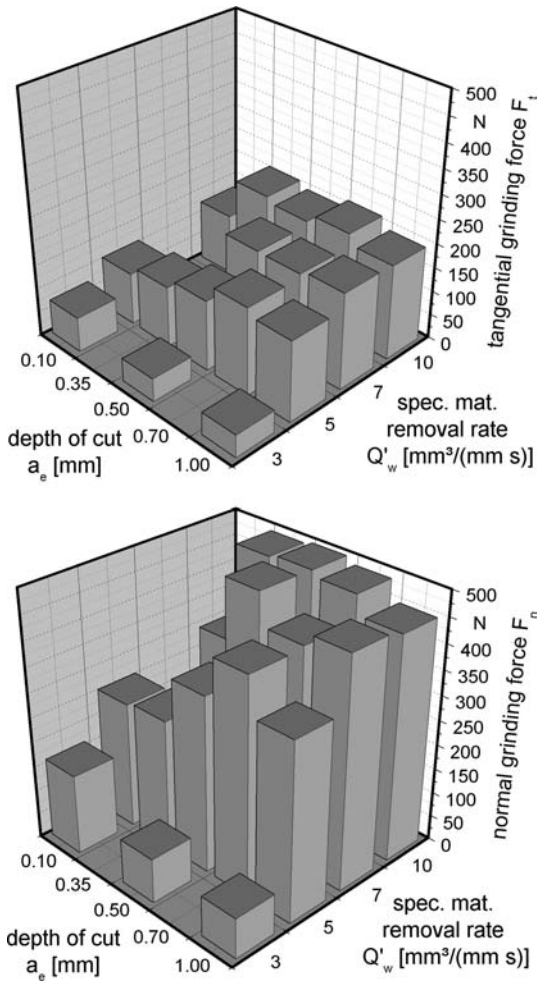


**Fig. 2** Measured tangential (*top*) and normal (*bottom*) grinding forces for different parameter sets

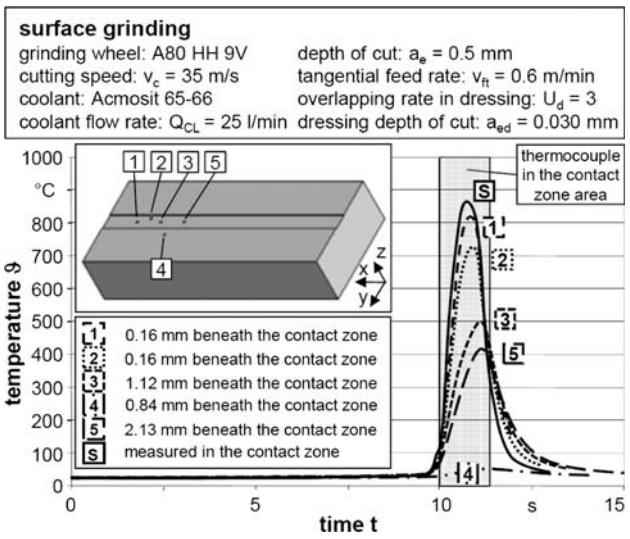


**Fig. 3** Temperature profiles measured in different distances from the contact zone

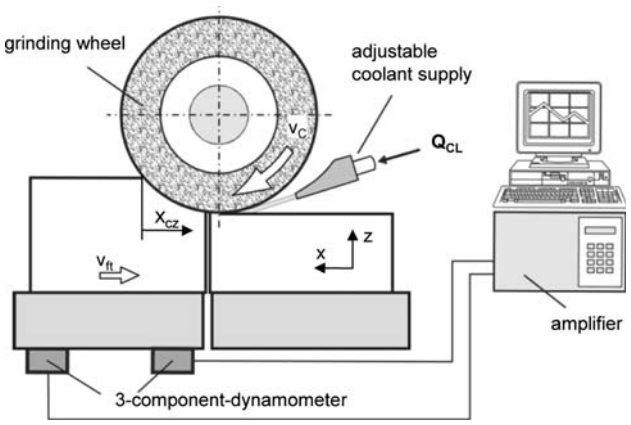


**Fig. 4** Illustration of the setup for the measurement of the tangential contact load

superimposed temperature curves for the five thermocouples relating to the mounting position of thermocouple 5 at a tangential feed rate of $v_{\mathrm{ft}} = 0.6$ m/min and a depth of cut of $a_e = 0.5$ mm.

## 2.2 Heat flux distribution

For the simulation of the temperature distribution in the workpiece the heat flux distribution in the contact zone is an important factor. The heat flux distribution describes the intensity of the heat source related to the contact zone area. In the literature often an idealized heat flux distribution is used. Common are constant, linear positive, linear negative, trapezoidal and parabolic heat flux distributions [3].

Based on the work of Shafto [4] and Schneider [5, 6] at IWT Bremen a test stand that offers the ability to measure the force distribution in the contact zone during grind-hardening was developed. From the force distribution in the contact zone the load profile and the effective heat flux distribution in feed direction could be derived. Basis of this procedure is the measurement of grinding forces from the time of the entrance of the grinding wheel into the workpiece up to the time of full engagement. For this purpose two workpieces are arranged behind one another in a distance of 50 µm, whereby the grinding wheel is with almost the entire contact length in engagement when entering the second workpiece (see Fig. 4).

A force measuring sensor attached under the second workpiece provides the distributions of the total tangential and to the total normal force, which represents the integral of all infinitesimally small tangential contact loads arising in the contact zone.

With consideration of the direction of the force components the total tangential force distribution is computed and approximated over a polynomial as accurately as possible. From the differential of the polynomial over the way the tangential contact load distribution $E_t$ ($x_{cz}$) results, with which the heat flux distribution can be computed directly. Figure 5 shows a typical total tangential force distribution $F_{\mathrm{t,total}}$ ($x_{cz}$) as well as the appropriate tangential contact load distribution $E_t$ ($x_{cz}$).

The measurements demonstrated that the largest tangential contact load occurs within the range of the maximum chip thickness and as a result the heat flux distribution in feed direction could be best approximated with a linear positive distribution. Thus, a linear positive heat flux distribution in feed direction was taken as the basis for all simulations. The heat flux distribution transverse to the feed direction was, based on the work of Noyen [7], regarded as almost constant.

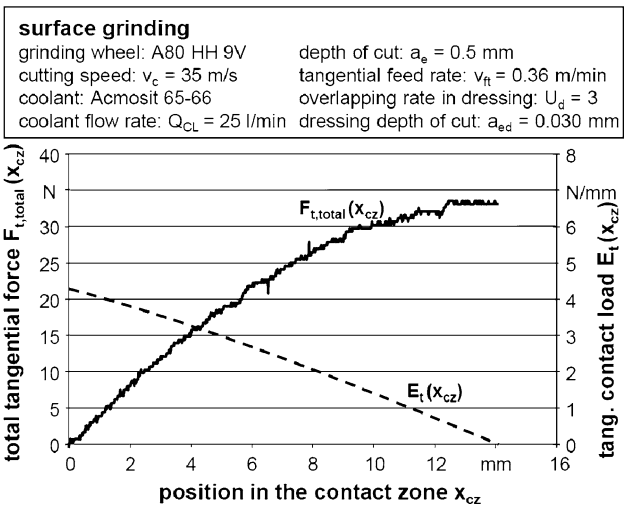


**Fig. 5** Total tangential force and tangential contact load during grind-hardening

### 2.3 Identification of the part distortions

For the comparison of experimental determined and numerical simulated part distortions during grind-hardening a basis of experimental results was needed, which was achieved by additional test series.

For this purpose, workpieces were machined with a length of 150 mm in grinding direction, a width of 28 mm and a height of 18 mm and with the parameters which were also used during the measurements of grinding forces and workpiece temperatures.

Before and after the grind-hardening operation the flatness of the workpieces was measured with a coordinate measuring machine.

Figure 6 depicts exemplarily the flatness deviation of a workpiece before and after the grind-hardening operation. For the comparison of different flatness deviations the peak-to-valley value (PV) is used.

The upper graph of Fig. 6 shows the nearly flat surface of the workpiece before the grind-hardening operation, whereas in the lower graph the distortion of the workpiece in feed direction after the grind-hardening operation is shown.

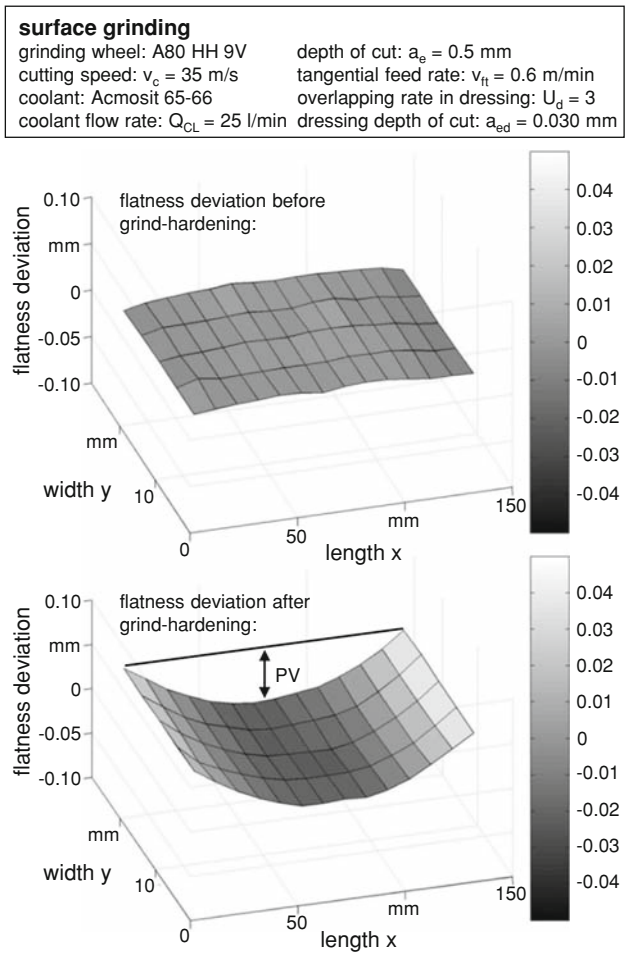


**Fig. 6** Workpiece flatness before and after grind-hardening (3D)

### 2.4 Hardness profiles and cross-section micrographs

Besides the mentioned measurements of grinding forces, temperatures and part distortions, micrographs and hardness profiles for each workpiece were made. Some of the results are shown in Sect. 3. The hardening depth is defined as the depth with a hardness of 80% of the surface hardness.

## 3 Realization of the simulation model and comparison with the measured results

As already mentioned above, the developed and implemented simulation method should be used to support the layout of the grind-hardening process. Therefore, the quality of the simulation model has to fulfill the requirements to predetermine the surface hardness, the hardening depth and the resulting part distortions numerically based on the applied parameter sets. The following chapters illustrate the modeling of the grind-hardening process including the deployed reduction methods according to Roeren [8] as well as the comparison and discussion of the measured and simulated results. All simulations are carried out using the tool “Sysweld” of the ESI Group.

### 3.1 Thermo-metallurgical model for the identification of the process parameters

The quality of the simulated results concerning the hardening depth and the surface hardness using a thermo-metallurgical model primarily depends on the calculated temperature field below the contact zone area. Therefore, the focus during the model buildup is set on this aspect concerning the steps meshing, modeling of the heat balance as well as the microstructural transformation within the surface layer. As a result of this, the material removal is not considered in the first instance. Otherwise, the importance of the thermo-metallurgical effects within the surface layer is considered by means of the fine discretization within the buildup of the finite element mesh shown in Fig. 7.

Regarding the simulated temperature field, the resulting heat balance within the workpiece is determined by the heat input using a heat source model and the heat abstraction by means of the defined heat transfer coefficients on the surface elements of the mesh. Based on the experimental results concerning the identification of the distribution of the total tangential force (Fig. 5), a heat source with a linear positive profile shown in Fig. 9 is used. Furthermore, the measured tangential grinding forces

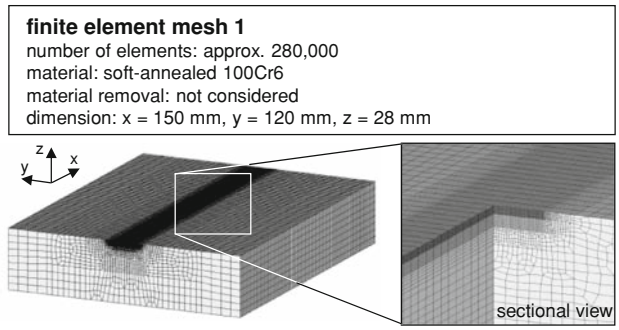


**Fig. 7** Finite element mesh 1

(Fig. 2) multiplied by the related heat distribution coefficient $K_w$ and the cutting speed provide a basis for the calculation of the heat input into the contact zone of the workpiece [3, 9–11]. As a result of the willful neglect of the material removal, the used heat distribution coefficients include all heat flows except for the heat abstraction via the chips and the grinding wheel.

Concerning the heat transfer coefficient at the surface of the workpiece, two zones are defined:

- Firstly, the coolant-overflowed area at the top side of the workpiece including the contact zone area, where heat transfer coefficients $h$ are pre-estimated extrapolating the results of Wittmann [12] and afterwards calibrated in relation to the heat distribution coefficient.
- Secondly, the other sides of the workpiece, where heat abstraction is dominated by the radiation over the surface.

These effects are described within the model using the analytical equations according to Baehr [13].

The heat transfer coefficient concerning the contact zone area and the heat distribution coefficient for different parameter sets resulting from the calibration of the simulation model are shown in Fig. 8. The calibration is based on the comparison of the measured and simulated temperature profiles as well as the hardening depth described in the following chapters.

Based on the time-dependent temperature distribution within the workpiece in conjunction with the description of the material model as well as the related material database of 100Cr6, the microstructural transformation within the surface layer can be calculated numerically. The diffusion-controlled transformations, e.g. from austenite to bainite, are modeled using the Johnson–Mehl–Avrami algorithm [14–18]. This algorithm is applied because the focus lies primarily on the modeling of the metallurgical effects of a heat treatment process [1, 8, 19], excluding the use of the simplified algorithm according to Leblond and Devaux[20].

Additionally, the non-diffusion-controlled lattice shearing, e.g. from austenite to martensite, is realized by means

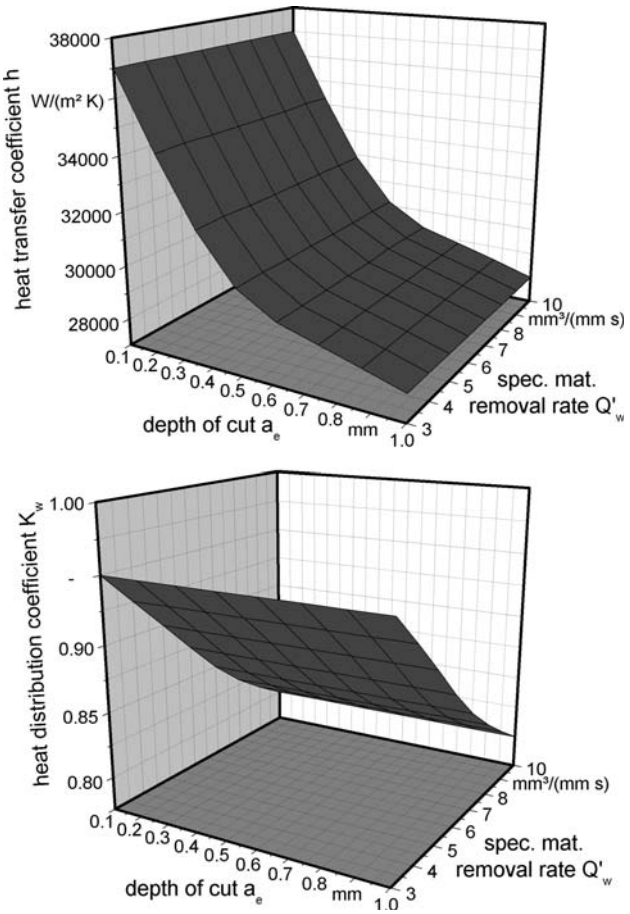


**Fig. 8** Heat transfer coefficient concerning the contact zone area (*top*) and heat distribution coefficient (*bottom*) used to calibrate the simulation model

of the Koïstinen–Marburger algorithm [21]. To build up and calibrate the material database as described in [18] and simultaneously taking the used algorithm into account, the required temperature-dependent data is provided by the time-temperature-transformation (TTT)-diagram, the continuous-cooling-transformation (CCT)-diagram and the time-temperature-austinitization (TTA)-diagram according to Wever et al. [22]. As initial value for the material of the simulated workpiece, the soft-annealed state of 100Cr6 (100% ferrit) is chosen.

### 3.2 Measured and simulated temperature distribution within the workpiece

As an example for a result of the thermo-metallurgical simulation of the grind-hardening process, Fig. 9 shows the simulated temperature field from the sectional view of the working plane and based on this the transient temperature profiles of the reference points defined in Fig. 3.

As already mentioned in [9], the temperature profiles as well as the maximal surface temperatures can only be used

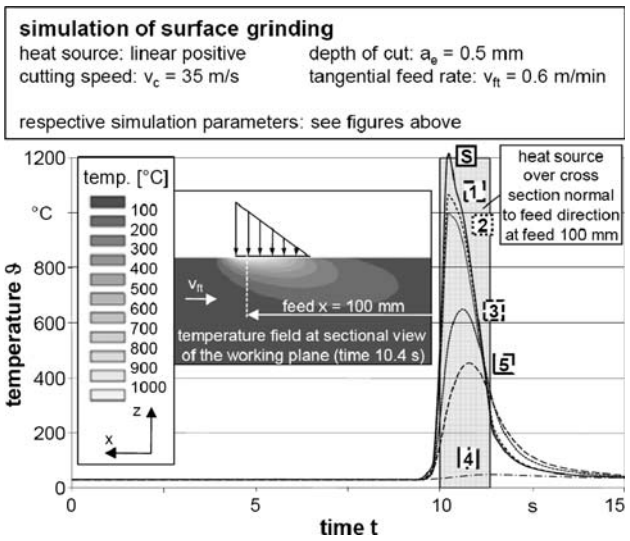


**Fig. 9** Simulated temperature field at the sectional view of the working plane as well as numerically calculated temperature profiles of the reference points according to the experiments (Fig. 3)

to achieve a qualitative evaluation compared to the measured results. Due to the fact that the focus of the calibration of the model is set on the hardening depth and the surface hardness, this effect is accepted consciously. An explanation is provided by the definition of the constitutive material equations, e.g. the TTA-diagram, on which the thermo-metallurgical simulation is based. Considering these interrelationships linked with the heating rates of the grind-hardening process, the calibration and the calculation of the model results in higher surface temperatures compared to the measured ones. These facts can be explained regarding the following two effects: Firstly, deviations within the measurements cause lower temperatures due to isolation effects between workpiece and thermocouples as well as influences of the coolant on the thermocouples. Secondly, concerning the simulation, the chosen material definition and database neglect the decrease of the austinitization temperature curve within the TTA-diagram based on the effect of pressure in the contact zone area mentioned by Maier [23].

The comparison of the measured and simulated surface temperatures for different parameter sets is shown in Fig. 10. As already mentioned above, the simulated surface temperatures are consistently higher than the measured ones, but the tendencies between those of the simulations and those of the experiments agree on many points concerning the corresponding parameter sets. The different simulated maximal surface temperatures with a depth of cut of 0.1 mm cannot be ensured yet because of the missing experimental results.

Concerning the area of the high surface temperatures, shown in Fig. 10, where the specific material removal rate

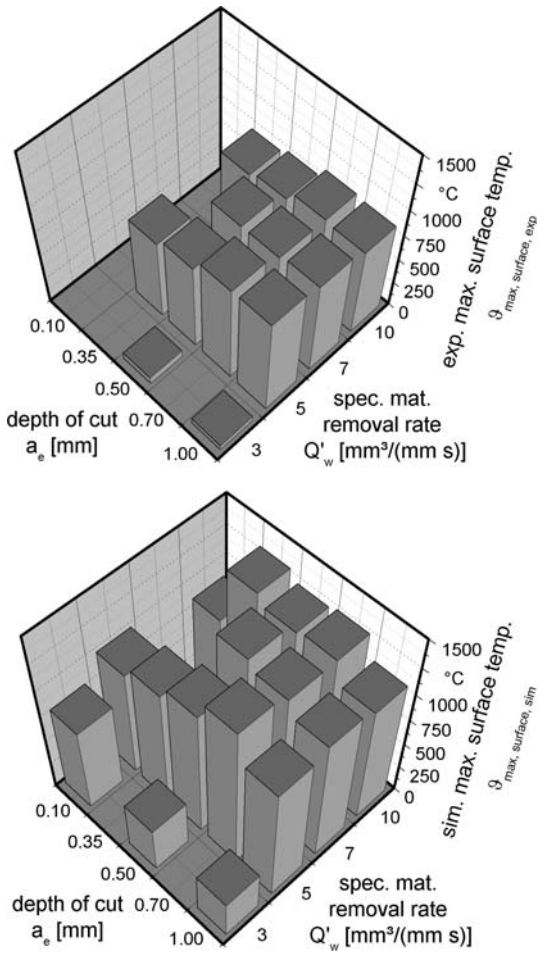


**Fig. 10** Maximal surface temperature concerning the experiments (*top*) and the simulation (*bottom*) for different parameter sets

is equal to or greater than 5 $mm^3/(mm\ s)$ and the depth of cut is equal to or greater than 0.5 mm, the diagrams reveal a range, where the machining by grinding enables a simultaneous surface hardening. This process window for the grind-hardening is also shown in Fig. 12, in which the measured surface hardness and the simulated hardening depth for different parameter sets are plotted.

### 3.3 Calculation of the microstructural transformation and the resulting surface layer hardness

Based on the simulated microstructural transformation linked with the cooling rates in the surface layer, the resulting hardness and hardening depth after cooling can be calculated. Figure 11 shows the measured and the simulated results concerning the hardening depth distributions for four different parameter sets. The pictured cross section views normal to the feed direction reveal the characteristic of the surface hardening and illustrate the location of the hardening depth distributions within the working plane as well as 1 mm and 3 mm outside of it.

Because of the high amount of carbon (1%) within the material 100Cr6, the method defined by Leslie [24] is used to calculate the hardness distribution of the surface layer. This method determines the hardness of soft-annealed 100Cr6 (100% ferrit) at 150 HV (Vickers hardness), which can be identified from the simulated hardening depth distributions (Fig. 11 left hand side). The maximal surface hardness of 825 HV as well as the constant distribution concerning the first layer under the contact zone area results from the simplifications due to the calculation of the microstructural transformation and the equation defined by Leslie [24].

Relating to the results shown in Fig. 11, the measured and simulated hardening depths match in many aspects. In addition to this, the distribution of the three curves in regard to their location in the contact zone area match well, especially for the parameter sets with a depth of cut of 0.5 mm. Generally, the curves represent the hardening depth distribution by lower hardening depths at 3 mm outside the working plane compared to the two other curves, which have consistently the same curve progressions. An exemplary hardening depth distribution is displayed by means of the cross section views at the top of Fig. 11.

The process window of the grind-hardening concerning the realized surface layer hardening can be seen in Fig. 12 based on the measured surface hardness and the simulated hardening depth. The measured surface hardness is diagnosed using the method defined by Rockwell [19] and

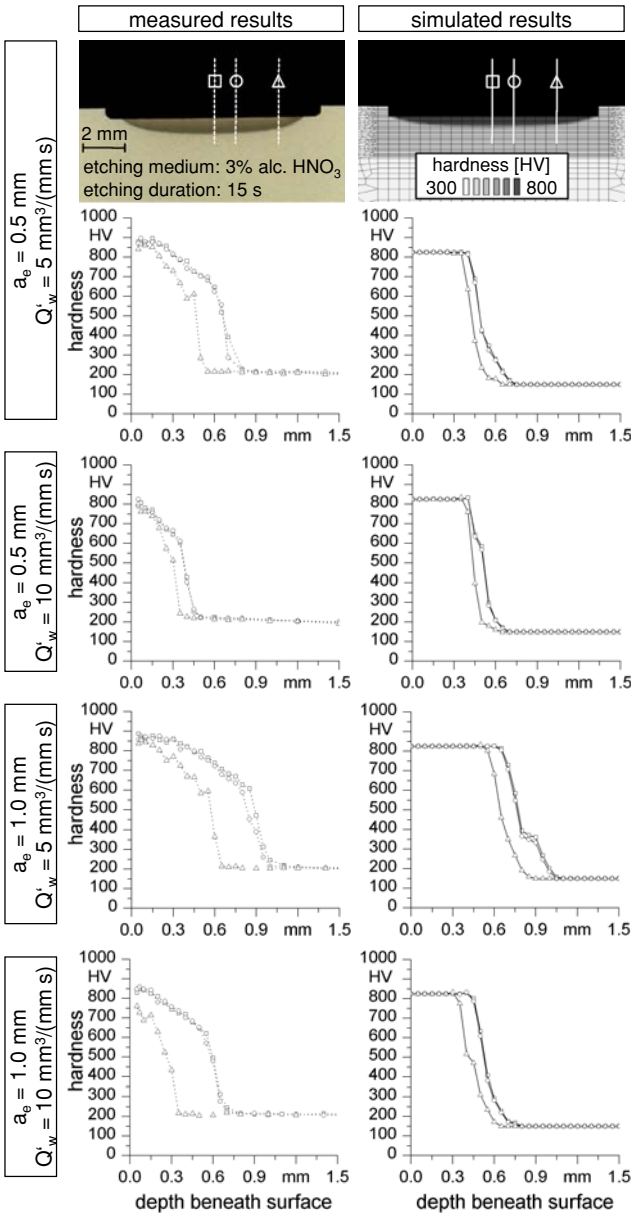


**Fig. 11** Comparison of the measured (*left*) and the simulated (*right*) results concerning the hardening depth distributions for four different parameter sets as well as the cross section views normal to the feed direction

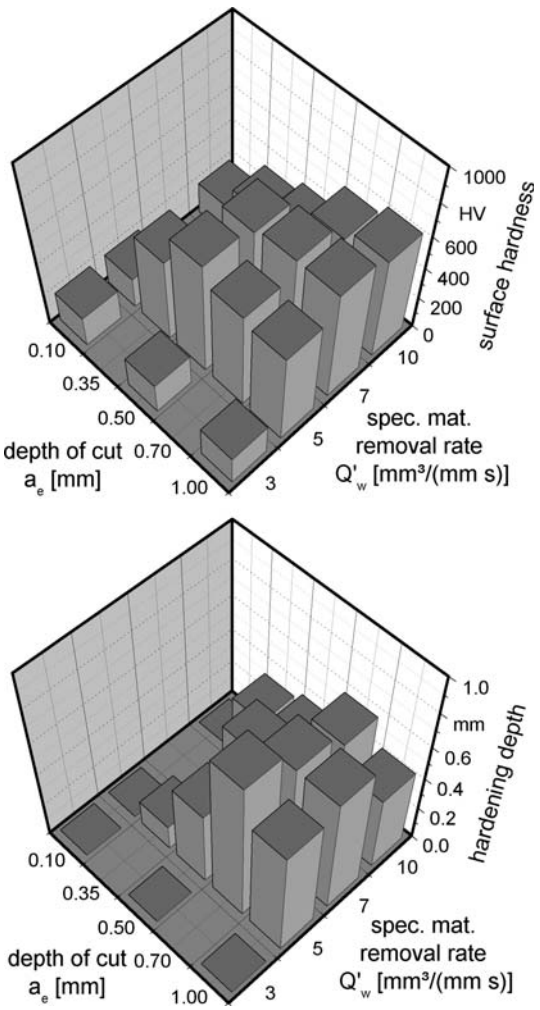


**Fig. 12** Measured surface hardness (*top*) and simulated hardening depth (*bottom*) for different parameter sets

afterwards translated to the Vickers hardness. Without any hardness penetration, the surface hardness is 190 HV, analogue to the measured hardening depth distributions in Fig. 11 at a distance from the part surface of 1.5 mm.

### 3.4 Simulation of the resulting part distortions

Based on the thermo-metallurgical simulation with its calculation of the heat balance within the workpiece and the resulting microstructural transformation within the surface layer, the thermo-mechanical simulation enables the numerical estimation of part distortions. The calculation of the mechanical behavior is an essential output quantity to evaluate the actual result of a grind-hardening process and is therewith a main aim of the cooperation within this project. To analyze the distortion behavior of a workpiece machined by means of a grind-hardening process a bar with a square cross-section is used, shown in Fig. 13. Analogue to the first finite element mesh, the effects and gradients within the surface layer at the contact zone area are considered by a fine discretization. The real mechanical behavior of the bar and the simultaneous disregarding of the material removal are appointed using the final geometry as initial state of the mesh.

Taking over the settings of the experiments, the mechanical boundary conditions, e.g. the clamping, are defined in two states, pictured in Fig. 13. Firstly, the magnetic fixture at the machine table during the grind-hardening process is regarded clamping all nodes of the bottom side of the finite element mesh. Secondly, considering the location after the machining and during the experimental examination of the distortion, the edges at the top side of the workpiece are clamped using a fixed-floating-bearing, shown in Fig. 13.

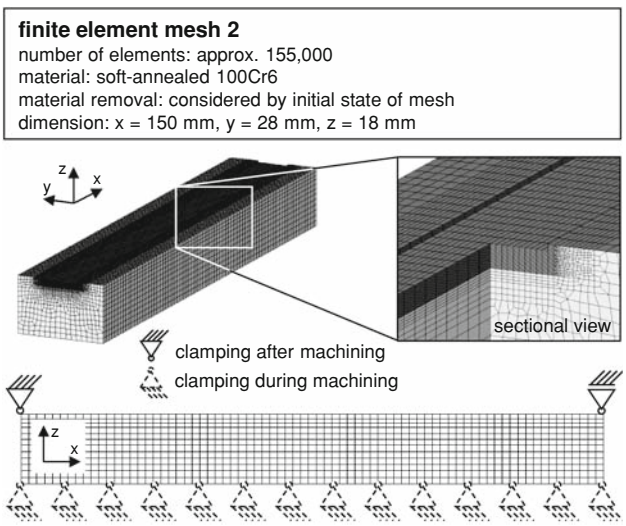


**Fig. 13** Finite element mesh 2 with clamping during and after the grind-hardening process

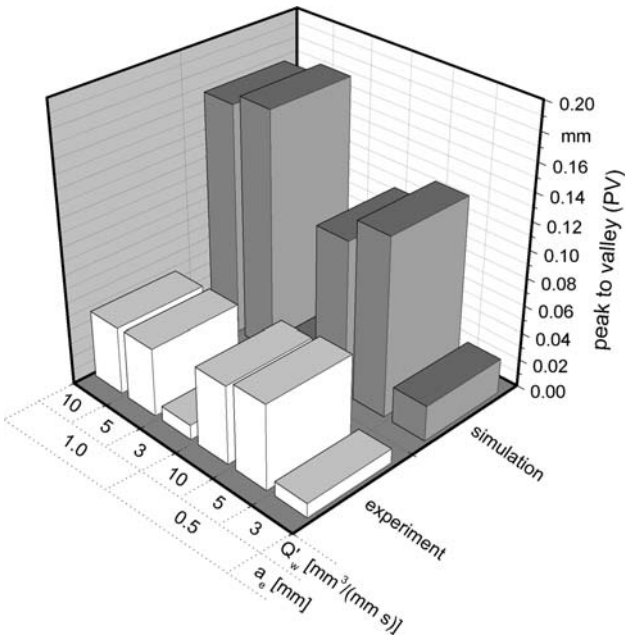


**Fig. 14** Comparison of the measured and simulated part distortions after cooling concerning the parameter peak-to-valley

According to the experiments, the examination of the distortion in z-direction is identified using nodes of the finite element mesh located at the cutting line of the bottom side and the working plane. The value peak-to-valley is defined analogue to the experiments.

Figure 14 shows the comparison of the measured and the simulated distortions after cooling concerning the peak-to-valley value. The distortions tend to show qualitatively matchable results due to the different parameter sets, but the simulated distortions are consistently higher than the measured ones. As mentioned by Wilke [25], the distortions as a result of the thermo-metallurgical effects of cutting processes depend on the heat input, the microstructural transformation and the pressures within the contact zone area based on the cutting forces. In this regard, the detected differences regarding the measured and the simulated distortions can be explained by neglecting the material removal and the pressures within the contact zone concerning the simulation model as well as the higher calculated temperatures within the surface layer compared to the experiments.

## 4 Conclusion

The research results of the thermo-metallurgical and the thermo-mechanical calculations presented within this paper illustrate the possibility to simulate the essential effects of

a grind-hardening process: the heat balance within the workpiece, the microstructural transformation and the hardness depth distribution within the surface layer as well as the qualitative resulting part distortions. Therewith, the FEA is generally qualified to identify the optimized range of the grind-hardening process concerning the above mentioned relevant aspects.

Future research activities will analyze the discussed divergences between measurement and simulation. The target-oriented optimizations of the simulation model should offer a possibility to handle the complex physical interrelationships of the grind-hardening process. Besides the implementation of the material removal and the pressures within the contact zone, a possible option for improvement is the adjustment of the TTA-diagram regarding the heating and transformation behavior of the grind-hardening process.

**Acknowledgments** The authors would like to thank the Deutsche Forschungsgemeinschaft (DFG) for funding the project BR 825/48-1/ZA 288/17-1: "Simulation of the Grind-Hardening Process". The results which were presented in this work are part of this project.

## References

1. Brockhoff T (1999) Schleifprozesse zur martensitischen Randschichthärtung von Stählen. Dr.-Ing. Dissertation University of Bremen. Shaker, Aachen
2. Brinksmeier E, Minke E, Wilke T (2005) Investigations on surface layer impact and grinding wheel performance for industrial grind-hardening applications. WGP Ann German Acad Soc Prod Eng 12(1):35–40
3. Brinksmeier E, Aurich JC, Govekar E, Heinzel C, Hoffmeister HW, Klocke F, Peters J, Rentsch R, Stephenson DJ, Uhlmann E, Weinert K, Wittmann M (2006) Advances in modeling and simulation of grinding processes. CIRP Ann Manuf Technol 55(2):667–696
4. Shafto GR (1974) Creep feed grinding. Bristol
5. Weinert K, Schneider M (2000) Simulation of tool-grinding with finite element method. CIRP Ann Manuf Technol 49(1):253–256
6. Schneider M (1999) Auswirkungen thermomechanischer Vorgänge beim Werkzeugschleifen. Dr.-Ing. Dissertation University of Dortmund. Vulkan, Essen
7. Noyen M (2008) Analyse der mechanischen Belastungsverteilung in der Kontaktzone beim Längs-Umfangs-Planschleifen. Dr.-Ing. Dissertation University of Dortmund. Vulkan, Essen
8. Roeren SR (2007) Komplexitätsvariable Einflussgrößen für die bauteilbezogene Struktursimulation thermischer Fertigungsprozesse. Dr.-Ing. Dissertation Technische Universitaet Muenchen. Utz, Munich
9. Zäh MF, Föckerer T, Brinksmeier E, Heinzel C, Huntemann J-W (2009) Experimentelle und numerische Bestimmung der Einhärtetiefe beim Schleifhärten. wt Werkstattstechnik online 99(1/2):49–55
10. Brinksmeier E, Heinzel C, Böhm C, Wilke T (2003) Simulation of the temperature distribution and metallurgical transformations in grinding by using the finite-element-method. WGP Ann German Acad Soc Prod Eng X(1):9–14
11. Chryssolouris G, Tsirbas K, Salonitis K (2005) An analytical, numerical, and experimental approach to grind-hardening. J Manuf Process 7(1):1–9
12. Wittmann M (2007) Bedarfsgerechte Kühlschmierung beim Schleifen. Dr.-Ing. Dissertation University of Bremen. Shaker, Aachen
13. Baehr HD, Stephan K (2006) Heat and mass transfer. Springer, Berlin
14. Johnson WA, Mehl RF (1939) Reaction kinetics in process of nucleation and growth. Trans Am Inst Mining Metall Pet Eng 135:416–458
15. Avrami M (1939) Kinetics of phase change. I—general theory. J Chem Phys 7:1103–1112
16. Avrami M (1940) Kinetics of phase change. II—transformation-time relations for random distribution of nuclei. J Chem Phys 8:212–224
17. Avrami M (1941) Kinetics of phase change. III—granulation, phase change and microstructure. J Chem Phys 9:177–184
18. N.N.: SYSWELD 2008—Welding and heat treatment reference manual. ESI Group 2007, Paris
19. Bargel H-J, Schulze G (2004) Werkstoffkunde. Springer, Berlin
20. Leblond JB, Devaux J (1984) A new kinetic model for anisothermal metallurgical transformations in steels including effect of austenite grain size. Acta Metall 32(1):137–146
21. Koïstinen DP, Marburger RE (1959) A general equation prescribing the extent of the austenite-martensite transformation in pure iron-carbovereinfachtn alloys and plain carbon steels. Acta Metall 7(1):59–60
22. Wever F, Rose A, Peter W, Strassburg W, Rademacher L (1961) Atlas zur Wärmebehandlung der Stähle Band 1. Stahleisen, Düsseldorf
23. Maier B (2008) Beitrag zur thermischen Prozessmodellierung des Schleifens. Dr.-Ing. Dissertation RWTH Aachen. Shaker, Aachen
24. Leslie WC (1982) The physical metallurgy of steels. McGraw-Hill, New York
25. Wilke T (2008) Energieumsetzung und Gefügebeeinflussung beim Schleifhärten. Dr.-Ing. Dissertation University of Bremen. Shaker, Aachen